Monte-Carlo simulations of star-branched polyelectrolyte micelles

M. Roger, P. Guenoun, F. Muller, L. Belloni, M. Delsanti

Eur. Phys. J. E **9**, 313–326 (2002)
DOI 10.1140/epje/i2002-10086-0

THE EUROPEAN PHYSICAL JOURNAL E

Monte Carlo simulations of star-branched polyelectrolyte micelles

M. Roger[1,a], P. Guenoun[1], F. Muller[1], L. Belloni[2], and M. Delsanti[2]

[1] DRECAM, Service de Physique de l'Etat Condensé, CEA Saclay, 91191 Gif-sur-Yvette Cedex, France
[2] DRECAM, Service de Chimie Moléculaire, CEA Saclay, 91191 Gif-sur-Yvette Cedex, France

Received 18 July 2002 and Received in final form 11 October 2002 /
Published online: 21 January 2003 –

Abstract. The concentration profiles of monomers and counterions in star-branched polyelectrolyte micelles are calculated through Monte Carlo simulations, using the freely jointed chain model. We have investigated the onset of different regimes corresponding to the spherical and Manning condensation of counterions as a function of the strength of the Coulomb coupling. The Monte Carlo results are in fair agreement with the predictions of Self-Consistent-Field analytical models. We have simulated a real system of diblock copolymer micelles of (sodium-polystyrene-sulfonate)(NaPSS)–(polyethylene–propylene)(PEP) with $f = 54$ hydrophilic branches of $N = 251$ monomers at room temperature in salt-free solution. The calculated form factor compares nicely with our neutron scattering data.

PACS. 82.70.-y Disperse systems; complex fluids – 61.20.-p Structure of liquids – 82.35.Rs Polyelectrolytes

1 Introduction

Charged diblock copolymers with a long and fully charged hydrophilic part and a short hydrophobic head are attracting a great attention. In water, their hydrophobic cores tend to aggregate and they form colloidal solutions of star-branched spherical micelles. These physical systems have many applications in surface adhesion, stabilization of colloidal solutions and are also used in drug delivery processes. Due to the presence of long-range Coulomb interactions, simple scaling arguments are generally unsufficient to describe their behavior. Quantitative predictions concerning the concentration profiles of monomers and counterions have been obtained through Self-Consistent-Field (SCF) models [1–3]. Numerical simulations can also provide useful information. The Molecular-Dynamics (MD) approach has been widely used in the study of neutral star-branched micelles [4] and charged linear polyelectrolytes [5,6]. Recently, Jusufi, Likos and Löwen (JLL) [7,8] applied it to star-branched polyelectrolyte micelles. They studied, at relatively low linear charge densities of the chains, the monomer and counterion profiles of one micelle and the effective interaction between two micelles. They also proposed analytical approximations to be compared with the results of MD simulations.

We focus here our attention on the problem of one isolated micelle, in a different strongly charged regime, which is relevant for some dilute solutions of (sodium-polystyrene-sulfonate)(NaPSS)–(polyethylene–propylene) (PEP) that have been investigated through neutron scattering in our laboratory [9].

We use the Monte Carlo method which, through a stochastic approach, should provide the same information as the Molecular Dynamics. Our final goal is to reach real-system sizes like stars with $f = 54$ arms of $N = 251$ monomers (27108 particles), corresponding to experimental conditions and to compare with our neutron scattering data, without any adjustable parameter. As a prelude, we first present a systematic investigation of smaller micelles within a more general theoretical framework and compare our numerical Monte Carlo results with the predictions of scaling theories and analytical approximations.

After the description of our model and Monte Carlo method (Sect. 2), we study in Section 3 the evolution of the structure of a micelle with $f = 27$ arms of $N = 130$ monomers as a function of the following dimensionless parameter measuring the strength of the Coulomb interaction:

$$\zeta = |z_{\rm i}|\xi = |z_{\rm i}||z_{\rm m}|l_{\rm B}/a, \tag{1}$$

where

$$l_{\rm B} = (e^2/4\pi\epsilon\epsilon_0)(1/k_{\rm B}T) \tag{2}$$

is the Bjerrum length, $\xi = |z_{\rm m}|l_{\rm B}/a$ represents the "Manning parameter" [10] which characterizes the linear charge density of polymers; a is the distance between consecutive charged monomers, T is the temperature, ϵ the dielectric constant of the solvent and $z_{\rm m}$, $z_{\rm i}$ represent the valence of monomers and counterions, respectively. Throughout our study $z = -z_{\rm m} = z_{\rm i} > 0$ and all monomers are charged.

[a] e-mail: roger@drecam.saclay.cea.fr

The Bjerrum length is $l_B \approx 0.71$ nm in water at room temperature and it can be varied through the temperature and dielectric constant. The monomer length is usually of the order of a fraction of a nanometer. ζ is approximately 3 for sodium polystyrene sulfonate in water. It can be increased by choosing other solvents with lower dielectric constants and/or by taking polyvalent monomers and counterions ($z > 1$). Higher values of ζ are thus easily accessible. Although in our fully charged model small values of ζ, much less than 1, are at present experimentally unrealistic, it is nevertheless interesting to extend our theoretical investigations down to that range.

When the thermal energy is much larger than the Coulomb interaction ($\zeta \ll 1$), most counterions are outside the micelle corona. This corresponds to the "unscreened regime" [1]. Above some threshold value $\zeta_{sph} \approx 1/f$, a spherical condensation of counterions inside and in the vicinity of the corona is expected [1–3,11]. In this so-called "osmotic regime" [1–3], the spherically condensed counterions lower the interaction between branches. Both unscreened and osmotic regimes have been extensively studied through mean-field analytical models [1–3,12]. Finally, when the "Manning criterion" [10] $\xi_M \approx 1/z_i$, *i.e.* $\zeta_M \approx 1$, is reached, a "cylindrical condensation" of part of the counterions around the branches is superimposed to the spherical condensation. Scaling and SCF theories [1–3,13] have predicted a linear extension of the branches with corona radius R_c proportional to N and monomer density varying roughly as $1/r^2$, where r represents the radial distance to the center of the micelle. This has justified a "rod-like" picture of the branches. This picture has been confirmed by clear experimental evidence of the stretching of the chains [14]. For highly charged polymers, a Poisson-Boltzmann analysis [15] has been proposed to interpret the distribution of counterions around the rod-like branches in terms of a ionic condensation [10,16].

In the three latter regimes, we have compared the results of our simulations to the expectations from approximate analytical theories. The simulation of a real system of (sodium-polystyrene-sulfonate)(NaPSS)–(polyethylene–propylene)(PEP) with $f = 54$ branches of $N = 251$ monomers, is described in Section 4, with a direct comparison to our neutron scattering data [9].

2 The model and Monte Carlo method

2.1 The model

We use the simple "freely jointed chain" (or "pearl necklace") model. Each monomer is represented by a hard core of diameter $\sigma_m = a$. The angle between two successive monomer-monomer segments is free. We consider that the hydrophilic chain is fully ionized in water and each monomer carries a charge ($z_m e$). This is relevant for sodium-polystyrene-sulfonate, in our experimental conditions, where the degree of ionization is generally of order 0.95. The counterions are modeled by hard spheres of diameter $\sigma_i = a/2$, and they carry a charge ($z_i e$). For sodium-polystyrene-sulfonate $z_i = -z_m = 1$.

One isolated micelle and the counterions are treated in the "primitive cell model", *i.e.* they are confined inside a hard-wall cube of edge A, surrounding the center of the micelle. The dielectric constant is assumed to be the same inside and outside the cubic cell. This approach is relevant for low concentrations with respect to the overlap concentration c^* of micelles. The weak dependence of our physical results on the size A of this cubic box (provided it is larger than the diameter of the micelle) means that a more sophisticated treatment of Coulomb interactions (*e.g.*, periodic boundary conditions and Ewald sums) is not required here.

The hydrophobic core is modeled by a hard sphere of radius R_{core} of order from 5 to $20a$. The hydrophilic parts are attached at fixed points chosen on this sphere. Two distributions of these fixed points have been considered:

- a random distribution,
- a regularized distribution with approximate equidistance between first-neighbor pairs.

The results obtained with these different distributions are practically identical and it is thus not useful to perform mean values of Monte Carlo results over different realizations of random distributions of points on the sphere.

All distances are expressed in units of the monomer length a and the strength of the Coulomb interaction compared to $k_B T$ is measured by the dimensionless parameter ζ defined in equation (1).

2.2 Monte Carlo moves

For a counterion, an elementary move is chosen at random in a cube of edge $\delta x \approx 10a$ centered around it.

For polymers we use the "pivot algorithm", which has been shown to satisfy ergodicity [17]. A monomer P is chosen at random, and a unit vector $\hat{u}$ is taken randomly in some solid angle $\delta\Omega$ centered about the axis defined by P and the next monomer $(P+1)$. A rigid rotation of random angle around $\hat{u}$ is applied to the part of the polymer going from $(P+1)$ to its end. However, beyond Manning condensation ($\zeta > 1$), such a pivot algorithm involving only the monomers becomes inefficient since many counterions are localized around each polymer and the cost in energy to move a group of monomers away from these counterions prohibits any Monte Carlo move.

To circumvent this problem, we have used the "partially clothed" pivot algorithm proposed by Gordon and Valleau [18]. Having chosen a pivot P and the corresponding end part of the polymer, we look for all counterions at a distance less than d of this polymer part (the distance from the polymer is defined as the distance to the closest monomer). Each of these counterions is rotated in block with the part of the polymer, with a probability $p \leq 1$. The detailed-balance equation is satisfied if, in the Metropolis scheme, we take as the probability of acceptance of the Monte Carlo move [18]

$$P_{acc} = \min\{1, (1-p)^{n_{new}-n_{old}} \exp\left[-(U_{new}-U_{old})/k_B T\right]\}, \quad (3)$$

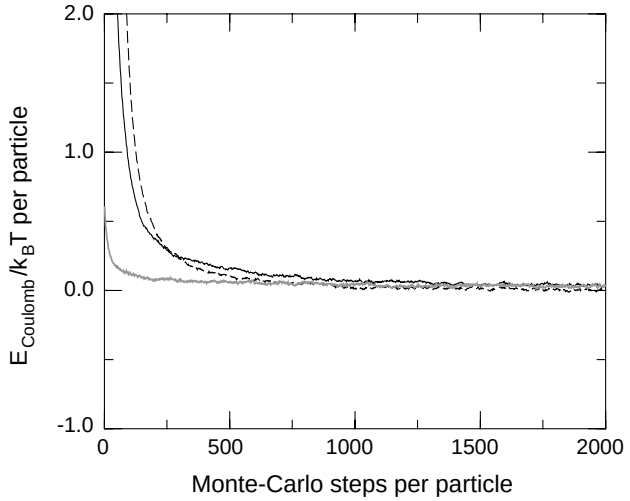

Fig. 1. Coulomb energy as a function of the number of steps at $\zeta = 2$. Full black line: starting from fully stretched polymers. Dashed line: starting from the configuration of neutral polymers. Full gray line: starting from the equilibrium configuration at $\zeta = 1$. Here $N = 130$, $f = 27$, $A = 320a$. Beyond 1000 steps, the differences between the three curves are of the order of the fluctuations.

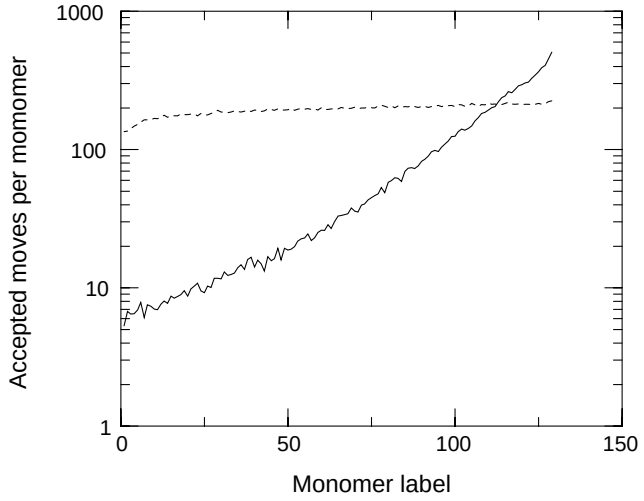

Fig. 2. Number of accepted "cluster moves" per monomer as a function of the monomer label (from 1 to N, starting from the core). Full line: "clothed pivot rotations"; dashed line: "clothed translations" (see text).

where $n_{\rm new}$ and $n_{\rm old}$ are the number of counterions at a distance less than d after and before the temptative rotation. $U_{\rm new}$ and $U_{\rm old}$ are the Coulomb energies after and before the trial move.

In practice, we have observed that "clothed pivots" have a reasonable probability to be accepted in the Metropolis scheme if $p > 0.9$. Since we did not observe very important differences in the convergence to equilibrium for $0.9 < p \leq 1$, we chose the value $p = 1$ which makes the algorithm simpler and the calculation shorter. (The choice $p = 1$ has also been made by Lobaskin and Linse [19] in similar "cluster moves" of macro-ions surrounded by a shell of small counterions). The maximum ion-polymer distance for clothed pivots has been optimized to $d = 4a$.

To facilitate stretching and contraction of the polymer, we have also applied some small "clothed block translations" of parts of polymer in the following way. A monomer P is chosen at random. The next monomer $(P+1)$ is moved from $\mathbf{r}_{(P+1)}$ to $\mathbf{r}'_{P+1}$ within a solid angle $\delta\Omega$ centered around $(\mathbf{r}_{(P+1)} - \mathbf{r}_P)$. The rest of the polymer from $(P+1)$ to its end is translated in block by a vector $(\mathbf{r}'_{(P+1)} - \mathbf{r}_{(P+1)})$. Such moves are also combined with "cluster moves" of counterions at a distance less than d. Compared to pivots they have a higher probability to be accepted and a suitable combination of these both types of cluster moves accelerates the convergence.

Our main criterion for equilibrium is the convergence of the Coulomb energy to the same stationary value starting from two drastically different initial configurations:

– Fully extended polymers with counterions distributed uniformly in the volume of the cell.

– Contracted star with polymers in the equilibrium configuration of uncharged polymer and counterions distributed uniformly in the volume of the cell.

As a typical example, Figure 1 illustrates the convergence of the Coulomb energy, starting from these two extreme configurations for a micelle with 27 branches of 130 monomers (2×3510 particles) at $\zeta = 2$. The equilibrium was reached after 10^3 steps per particle, representing 25 hours of monoprocessor time on a Compaq RS232 parallel computer. The relevant statistical properties (distribution of monomers and counterions, form factors, etc.) were measured over 10^3 further steps. A "cluster move" of a polymer part was attempted every 3 iterations (the two others being devoted to single counterion moves). The cluster moves were either pivots (3/4 of them) or translations (1/4 of them) as previously described. During the measure of statistical averages, each counterion was moved approximately 1300 times, about 80 pivots and 200 translations per monomer were accepted.

The number of accepted pivots as a function of the position of the pivoting point P is represented in Figure 2. Close to the core of the micelle, the number of accepted moves is low (of the order of 10 per monomer). Nevertheless, it grows roughly exponentially as a function of the position of monomer P and the statistics becomes acceptable beyond a few tens of monomers.

The size δx of the cubic box for elementary counterion displacements was $10a$, and the elementary solid angle $\delta\Omega$ for pivot rotations was fixed to $2\pi \cdot 10^{-2}$ steradians. We have also tried some simulation with $\delta\Omega$ increasing with the distance to the core of the micelle, without any substantial improvement of the rate of convergence to equilibrium.

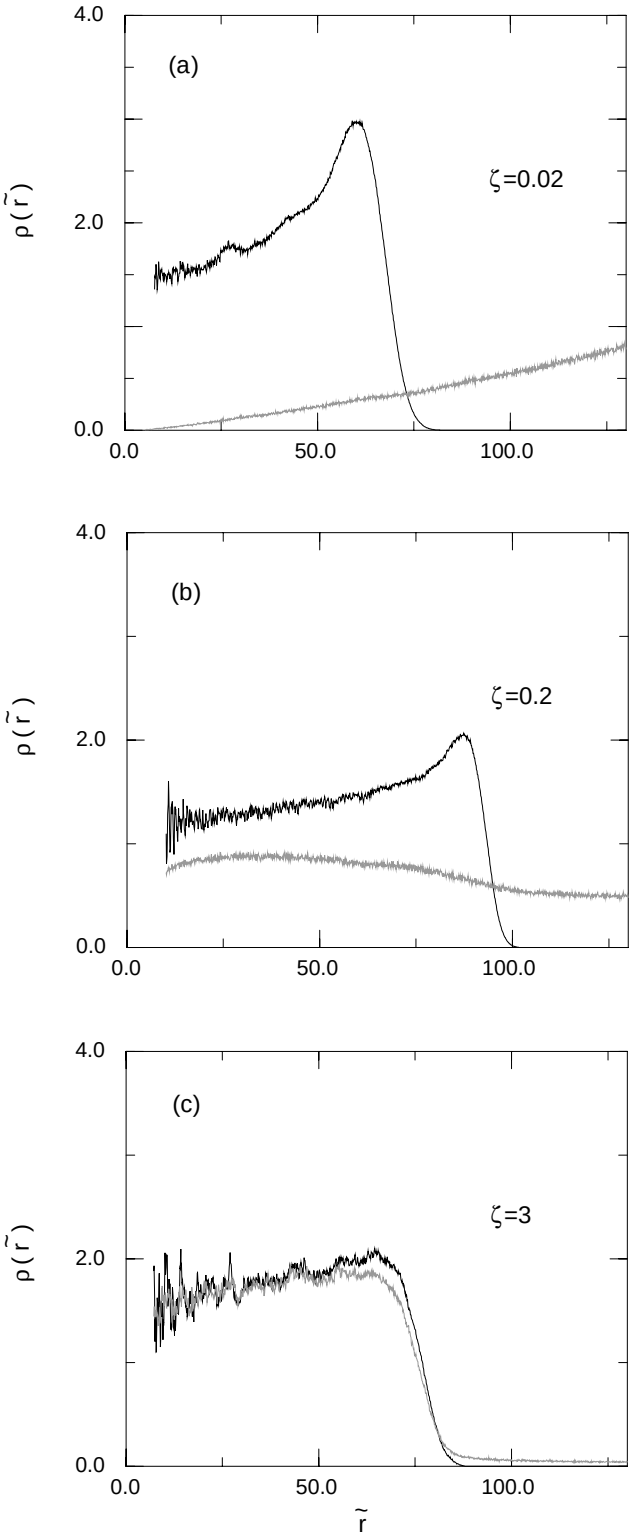

Fig. 3. Density profiles of monomers (black) and counterions (gray) in the three different regimes: (a) uncondensed regime ($\zeta = 0.02$); (b) spherically condensed regime ($\zeta = 0.2$); (c) Manning condensed regime ($\zeta = 3$). Here $N = 130$, $f = 27$ and $\tilde{A} = 320$.

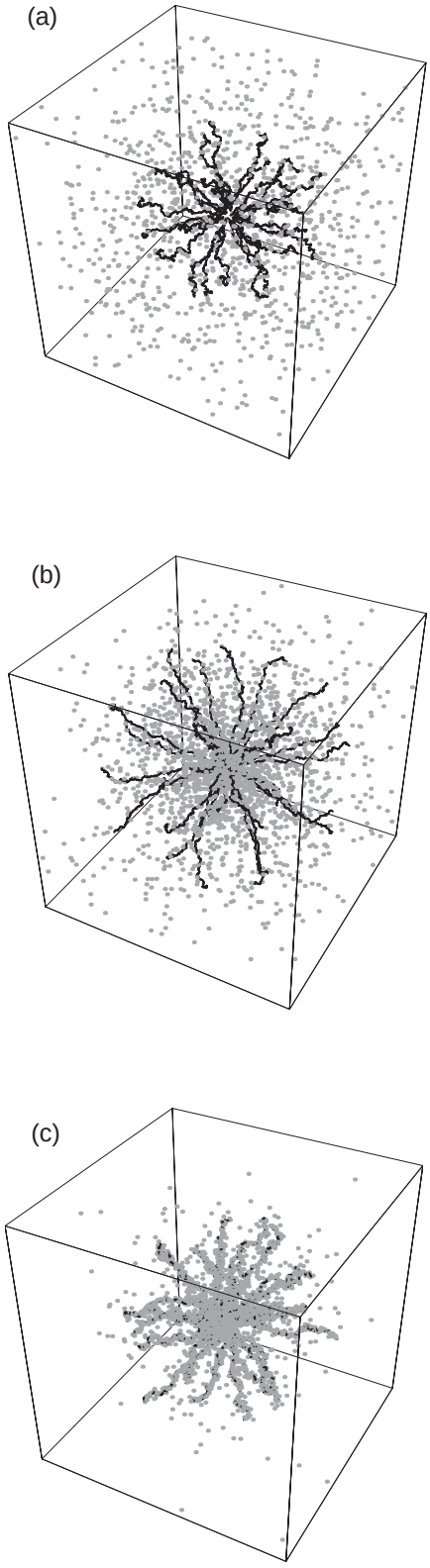

Fig. 4. Snapshots of the micelle in equilibrium corresponding to the three regimes considered in Figure 3, respectively. The three snaphots are represented at the same scale.

3 General results

3.1 The theoretical model studied

We present here some theoretical results concerning the variations of the monomer and counterion profiles as a function of the dimensionless parameter ζ (*cf.* Eq. (1)) measuring the strength of the Coulomb interaction with respect to $k_{\rm B}T$.

We consider two micelles with numbers of monomers and branches smaller than these corresponding to the experimental system studied in the next section:

i) $N = 130$ and $f = 6$;
ii) $N = 130$ and $f = 27$.

The radius of the core $R_{\rm core}$ is chosen to be small compared to the radius of the micelle corona and has thus a little influence on the corona. We take in all cases $R_{\rm core} = 5a$. The influence of the boundary conditions was investigated by comparing the results obtained with two different sizes of the cubic cell: $A = 320a$ and $A = 640a$.

We vary the dimensionless parameter ζ keeping the ratios $\tilde{A} = A/a$, $\tilde{R}_{\rm core} = R_{\rm core}/a$ and $\tilde{\sigma}_{\rm i} = \sigma_{\rm i}/a$ constant. We start from a low value $\zeta_0 = 0.005$ and increase it by steps. At each new step ζ_{n+1} we take as initial state of the Monte Carlo calculation the equilibrium state obtained at the preceding one ζ_n. The system is thus progressively "annealed", which provides a faster convergence to equilibrium at each step. As a typical test for equilibrium we compare in Figure 1 the energy obtained in that way at $\zeta = 2$ starting from the equilibrium configuration at $\zeta = 1$ to the results obtained with far-from-equilibrium arbitrary initial configurations. After 1000 iterations, the differences between all curves are of the order of the fluctuations.

We calculate the mean values of the radial distributions of monomers and counterions. The deviations of these distributions from the monomer distribution corresponding to fully extended arms are better emphasized by considering, in terms of $\tilde{r} = r/a$, the dimensionless quantities

$$\rho_{\{m,i\}}(\tilde{r}) = \frac{4\pi}{f}\tilde{r}^2 a^3 c_{\{m,i\}}(\tilde{r}), \qquad (4)$$

where $c_{\{m,i\}}(\tilde{r})$ represent the local volume densities.

For a micelle with fully extended arms, $\rho_{\rm m}$ should be 1 for $\tilde{R}_{\rm core} < \tilde{r} < \tilde{R}_{\rm core} + N$ and 0 elsewhere.

3.2 Monomer profile as a function of ζ

For $N = 130$, $f = 27$ and $\tilde{A} = 320$, typical monomer and counterion profiles are represented in Figures 3a, b and c at weak coupling ($\zeta = 0.02$), intermediate coupling ($\zeta = 0.2$) and strong coupling ($\zeta = 3$), respectively. Corresponding snapshots of the micelle are shown in Figure 4.

The variations of the radius of gyration $R_{\rm g}$ and of the corona radius $R_{\rm c}$ as a function of ζ are shown in Figure 5 (circles). The corona radius $R_{\rm c}$ is defined here as the abscissa of the maximum of the free-end distribution, which is approximately Gaussian (see Fig. 6). It also roughly coincides with the rightmost inflexion point in the concentration profile $\rho_{\rm m}(\tilde{r})$.

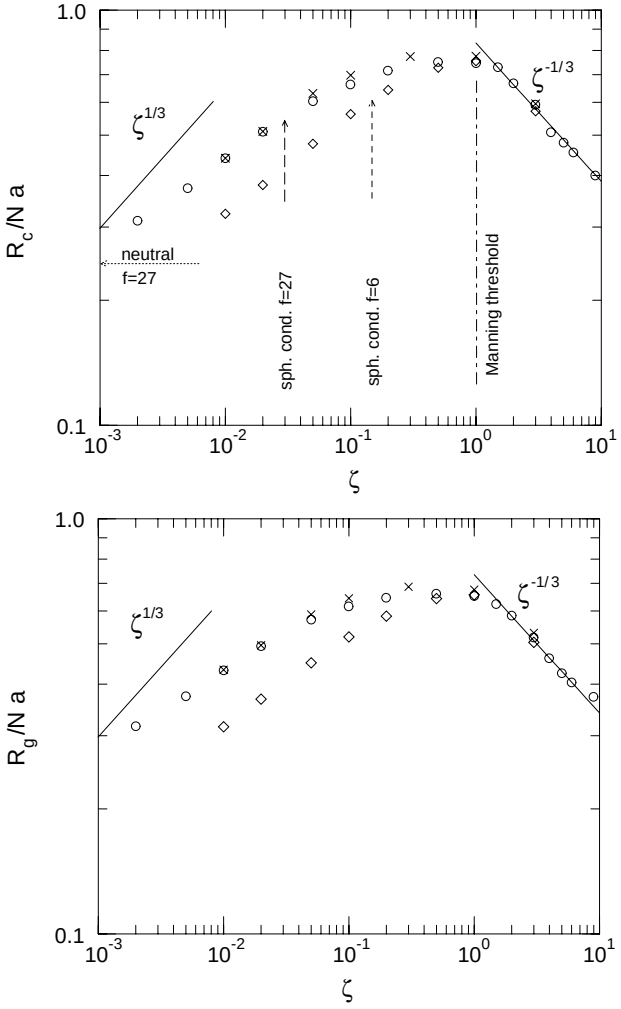

Fig. 5. Variation of the corona radius $R_{\rm c}$ and radius of gyration $R_{\rm g}$ as a function of the dimensionless parameter ζ for: i) $f = 27$, $\tilde{A} = 320$ (circles); ii) $f = 27$, $\tilde{A} = 640$ (crosses); iii) $f = 6$, $\tilde{A} = 320$ (diamonds). $N = 130$ in all cases. The Manning threshold is indicated by the dash-dotted vertical line $\zeta \approx 1$. The long-dashed and short-dashed vertical lines indicate different threshold values for spherical condensation corresponding to i), and iii), respectively . The horizontal arrow on the left indicate the limiting values of the corona radius corresponding to neutral stars with $f = 27$ arms of $N = 130$ monomers.

We have studied the influence of boundary conditions by doubling the size A of the cubic cell (crosses). $R_{\rm c}$ and $R_{\rm g}$ are very weakly dependent on boundary conditions. Relative differences of the order of a few percent at most are observed at maximum stretching (ζ of order 1). We conclude that it is not useful to investigate more sophisticated treatments of Coulomb interaction like these corresponding to periodic boundary conditions with Ewald sums.

The influence of the number of arms is seen in Figure 5 by comparing our results with a small number of arms

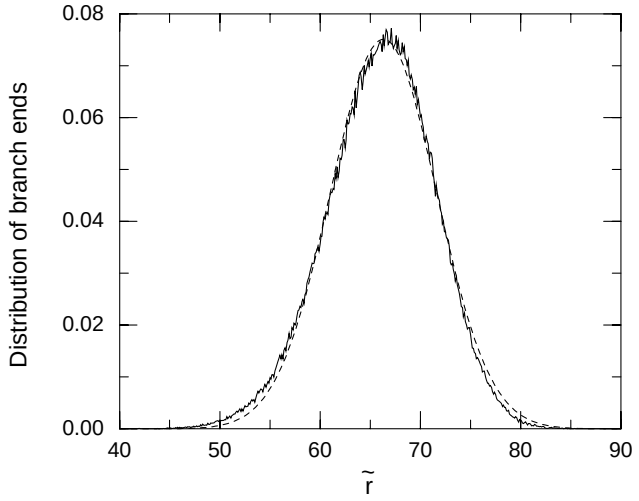

Fig. 6. Distribution of branch ends for $\zeta = 0.02$. The Monte Carlo results (full line) are fit by a Gaussian (dashed line): $1/[\sqrt{2\pi}(\tilde{\sigma})] \exp[-(\tilde{r}-\tilde{R}_c)^2/2\tilde{\sigma}^2]$ with $\tilde{R}_c = 66.33$ and $\tilde{\sigma} = 5.31$.

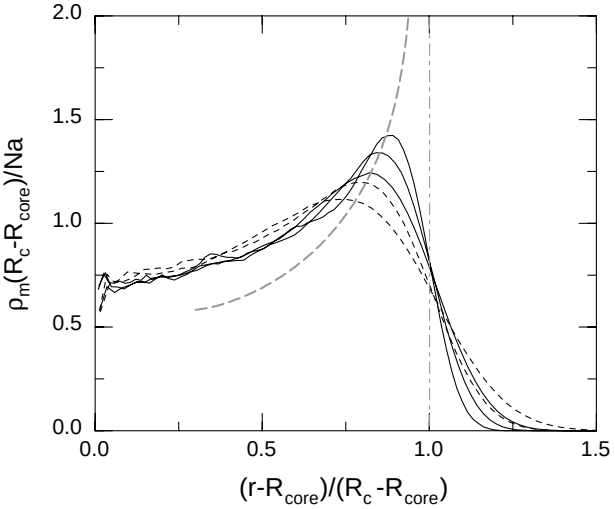

Fig. 7. Monomer profiles in the "unscreened" regime. Full lines: $N = 130$ and $f = 27$ for three ζ values, $\zeta = 0.005$ (lowest maximum), $\zeta = 0.01$ and $\zeta = 0.02$ (highest maximum). Short-dashed lines: $N = 130$ and $f = 6$ for $\zeta = 0.01$ and $\zeta = 0.02$. The gray dashed line indicates the solution of equation (7).

$f = 6$ (diamonds) to the results with $f = 27$ (circles). It is only important at weak coupling.

Figures 3, 4 and 5 show clearly, as a function of ζ, three different regimes. These three regimes are governed by changes in the behavior of the counterions, which are expected from mean-field theories [1–3,10,11].

3.3 The "unscreened regime"

At weak coupling $\zeta \ll 1$, the contribution of the counterions to the entropy dominates the electrostatic energy. The local volume density c_i of counterions is roughly constant in the cell: $c_i \approx fN/A^3$ and from equation (4) $\rho_i \approx 4\pi N\tilde{r}^2/\tilde{A}^3$. If A is larger than R_c, the fraction of counterions in the micelle corona is small and the electrostatic interactions between branches are weakly screened.

In the unscreened limit, the self-consistent field arguments proposed a long time ago for linear polyelectrolytes by de Gennes *et al.* [13] have been straightforwardly generalized to star-branched polyelectrolytes [1,2]. Let us consider a chain whose first unit is placed at the origin. The n-th unit is at an average distance $r(n)$ and feels two forces:

– In a simple Gaussian model, there is an elastic force which tends to contract the chain:

$$F_e = \frac{3k_BT}{a^2}\frac{d^2r}{dn^2}. \quad (5)$$

– If we assume equal stretching of the f chains of a star, *i.e.* all chain ends are at the same distance R_c from the origin, the spherical region at a distance smaller than $r(n)$ contains a mean charge $Q = nfz_me$. Applying Gauss theorem, there is an electrostatic force

$$F_c = \frac{nf(z_me)^2}{4\pi\epsilon\epsilon_0}\frac{1}{r(n)^2}. \quad (6)$$

Writing the equilibrium between the two forces, one obtains the following dimensionless equation:

$$\frac{d^2u}{dx^2} + \frac{1}{3}\frac{x}{u^2} = 0 \quad (7)$$

with $x = n/N$ and $u = r/(Nd)$, where the length scale d is

$$d = a\left(\frac{fz_m^2 l_B}{a}\right)^{1/3}. \quad (8)$$

The boundary conditions are $u(0) = 0$ and $du/dx = 0$ at $x = 1$. Taking $f = 1$ in the previous algebra is nothing else than de Gennes *et al.*'s equations [13].

The center-to-end distance of the chains is thus proportional to Nd:

$$R_c \approx f^{1/3}\zeta^{1/3}Na \quad (9)$$

(we take $z_i = -z_m$).

These simple scaling arguments lead to a stretching of the chains which is proportional to the number N of monomers. They have justified a so-called "rod-like" picture of the branches.

In Figure 5, the slope $d\log R_c/d\log\zeta$ is smaller than 1/3, the value expected through the previous scaling arguments. The dependence of R_c on f is also weaker than predicted by equation (9). At very weak coupling, we obtain (see Fig. 5) $R_c(f = 27)/R_c(f = 6) \approx 1.35$ compared to the expected scaling: $(27/6)^{1/3} = 1.65$. The explanation is that when ζ is low enough to ensure that very few counterions are inside the corona, the excluded-volume effects (which are not taken into account in the previous scaling arguments) become significant. The value of R_c has a lower limit which is given by the scaling law for neutral stars [20]:

$$R_c^{\text{neutral}} \approx af^{1/5}N^{3/5}. \quad (10)$$

This limiting value for $N = 130$ and $f = 27$, within our pearl necklace model is indicated in Figure 5. Our lowest value for R_c shows an inflexion towards this asymptote.

Close to the core, our monomer profiles can be roughly scaled on a universal curve by plotting $\rho_m(R_c - R_{core})/Na$ as a function of $(r - R_{core})/(R_c - R_{core})$ (*i.e.* the integral of each curve is normalized to 1) and compared to the solution of equation (7) given in Figure 2 of reference [1] (see Fig. 7). Close to the core, our Monte Carlo results agree qualitatively with the solution of equation (7) which gives a roughly constant profile of ρ_m (*i.e.* $a^3 c_m(\tilde{r}) \approx \tilde{r}^{-2}$). At R_c, equation (7) leads to some unphysical divergence, which is smoothed in more refined SCF models taking into account the fluctuations of the chain ends [1,3]. Nevertheless, a substantial increase of ρ_m near R_c remains in these SCF models, as well as in our simulation.

3.4 The "osmotic regime" with spherical condensation of counterions

Increasing ζ we expect a "spherical condensation" of a part of the counterions inside and in the vicinity of the corona. This occurs when the Coulomb energy of a counterion in the field created by the charged monomers,

$$(z_m N f) z_i e^2/(4\pi\epsilon\epsilon_0 R_c),$$

at the limit of the corona radius is of the order of kT, *i.e.* for

$$\zeta_{sph} \approx \frac{1}{f}$$

(at this level of approximation we take $R_c \approx Na$). The condensation of ions near the surface of an impenetrable charged sphere [11] has been formulated in an analogous way to the cylindrical condensation of ions around a charged rod studied by Manning [10]. The more complex problem of counterion condensation in a penetrable micelle has been studied through Self-Consistent Field methods [1–3]. It can also be formulated in a simpler way through a Poisson-Boltzmann analysis. The Poisson-Boltzmann equation can be solved numerically for a penetrable sphere of radius R_c with charge density

$$c_m(r) = fN/(4\pi R_c r^2) \qquad (11)$$

inside a spherical cell of volume A^3. Figure 8 compares the Monte Carlo to the Poisson-Boltzmann results for the osmotic coefficient ϕ. The osmotic coefficient is defined as the ratio of the osmotic pressure to its value corresponding to a uniform repartition of the ions in the cell. The osmotic pressure is equal to $k_B T$ times the local ionic density at the edge of the cell.

There is a clear change of slope of $\phi(\zeta)$ at a point which can be defined as the crossover to the condensed regime. For different numbers of arms and cell sizes, we deduce the crossover to the spherically condensed regime at the following values ζ_{sph}:

- $\zeta_{sph} \approx 0.15$ for $f = 6$, $\tilde{A} = 320$,
- $\zeta_{sph} \approx 0.03$ for $f = 27$, $\tilde{A} = 320$,
- $\zeta_{sph} \approx 0.08$ for $f = 27$, $\tilde{A} = 640$

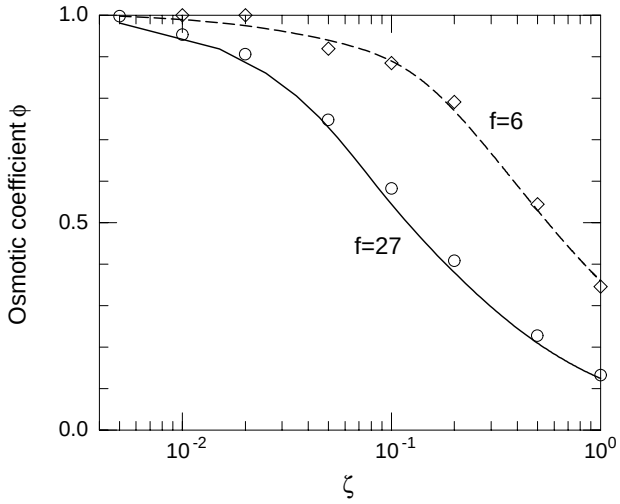

Fig. 8. Osmotic coefficient ϕ. The open diamonds and circles represent the Monte Carlo results for $f = 6$ and $f = 27$, respectively. The full and dashed line correspond to the Poisson-Boltzmann approximation. In both cases $\tilde{A} = 320$ and $N = 130$.

($N = 130$ in the three cases). At fixed $\tilde{A}$, ζ_{sph} varies in $1/f$.

In Figure 9, we show that at the thresholds defined above, there is a drastic change of the counterion profile. Below ζ_{sph}, the local density c_i of counterions is roughly constant $c_i \approx fN/A^3$ leading to a quadratic behavior of ρ_i. Above the threshold, the curves ρ_i show an inflexion point at $\tilde{r} \approx R_c/a$. Since in that ζ range R_c is roughly constant, the abscissa of this inflexion point remains constant.

For $\zeta \gg 1/f$, most of the counterions are inside the micelle corona (see Fig. 9). This regime has often been called "osmotic" by reference to the osmotic pressure of counterions inside the corona [2,3]. Neglecting the fraction of uncondensed counterions and writing at a chain end the equilibrium between the stretching force: $F_{osm} = k_B T N/R_c$ due to the osmotic pressure of counterions inside the star and the elastic force in the chain: $F_{el} \approx k_B T R_c/(Na^2)$ one obtains [2,3]: $R_c \approx Na$. Within these approximations, R_c is independent of f and ζ. In our Monte Carlo results (see Fig. 5), the range $1/f \ll \zeta < 1$ corresponds to the largest stretching of the star with a flat maximum in the curve $R_c(\zeta)$.

3.5 The "Manning condensed" regime

For larger ζ values, beyond the "radial condensation" of counterions in the micelle corona, we expect the superposition of a "cylindrical condensation" of counterions around each branch of the micelle. This phenomenon is clearly seen in Figure 3c and Figure 4c. The Manning criterion for this "cylindrical condensation" is [10,11]:

$$\xi_M = 1/|z_i|,$$

which corresponds to the threshold value $\zeta_M = 1$.

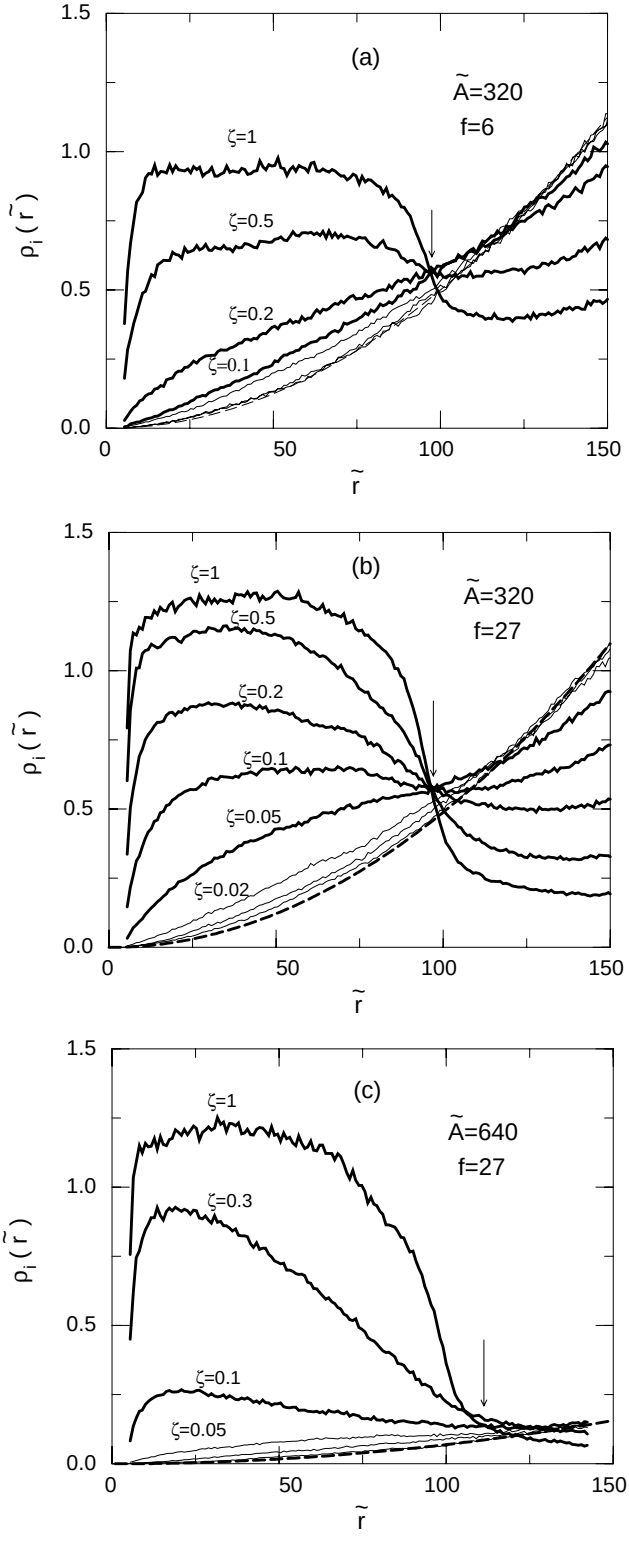

Fig. 9. Radial distribution of counterions ($N = 130$) as a function of ζ for different numbers of arms: (a) $f = 6$ and $\tilde{A} = 320$, (b) $f = 27$ and $\tilde{A} = 320$, and different cell sizes: (c) $f = 27$ and $\tilde{A} = 640$. The arrows indicate a common inflexion point at $r \approx R_c$ in the pure spherically condensed regime. The dashed parabolas indicate the equipartition of all counterions in the volume of the cell in the uncondensed regime.

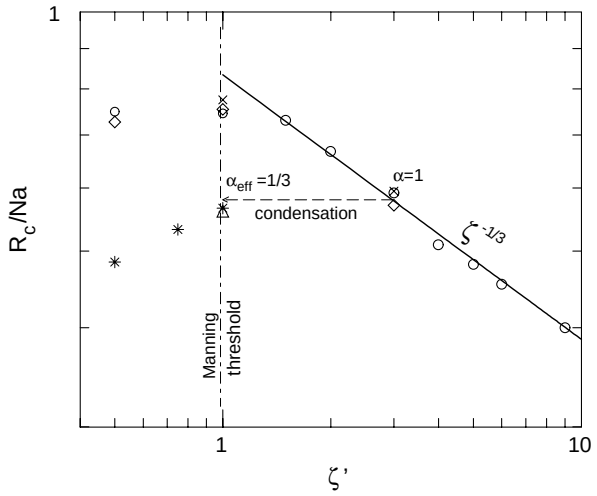

Fig. 10. Variation of the corona radius near and in the Manning condensed regime. The stars represents the results of JLL [7] for $N = 50$ and $f = 18$ at charge fraction $\alpha = 1/6$, $1/4$, $1/3$, the triangle corresponds to their results for $N = 150$, $f = 10$ and $\alpha = 1/3$, the abscissa is $\zeta' = \alpha\zeta$. In JLL [7], all simulations are at constant $\zeta = 3$. The other symbols are our results reported in Figure 5 with the same conventions (in our study α is fixed to 1 and $\zeta = \zeta'$ is varied). The dashed arrow indicates a mapping of our model at $\zeta = 3$ and $\alpha = 1$, in the strongly condensed Manning regime, onto an effective condensed system with charge fraction $\alpha_{\rm eff} = 1/3$. It agrees nicely with the real system at $\alpha = 1/3$ studied by JLL at the same $\zeta = 3$.

Figure 10 represents an enlargement of the last decade in Figure 5. The corona radius R_c presents a flat maximum at $0.5 < \zeta < 1$ and decreases at $\zeta > 1$. At this stage, it is interesting to compare our approach with the Molecular-Dynamics study by JLL [7,8], where ζ has been fixed to 3, but where only one monomer out of three, four or six is charged. The "charge fraction" α is thus varied from $\alpha = 1/3$ to $\alpha = 1/6$, whereas it is $\alpha = 1$ in our model. The relevant Manning parameter which characterizes the linear charge density of the polymer is $\xi = z_m l_B/b$, where $b = a/\alpha$ is the distance between consecutive charged monomers [21]. In Figure 10 we have plotted some of JLL results, as a function of $\zeta' = \alpha\zeta$. The fact that from $\alpha = 1/6$ to $\alpha = 1/3$ their corona radius increases, indicates that they have not reached the Manning condensed regime at $\alpha = 1/6$ and $\alpha = 1/4$. They are just reaching it near $\alpha = 1/3$.

At $\zeta \gg 1/f$ (near the broad maximum of R_c and in the Manning condensed regime), the monomer profiles are only very weakly dependent on f. In Figure 11, we compare the monomer profiles for different values of the number of branches $f = 6$, 27, and 54. The number of monomer per branch is $N = 130$, the radius of the hydrophobic core is $\tilde{R}_{\rm core} = 5$ and the size of the cell is $\tilde{A} = 320$. Figure 12 represents the variation of the gyration radius as a function of the number of branches f. It increases only by a few percent when the number of branches vary by a

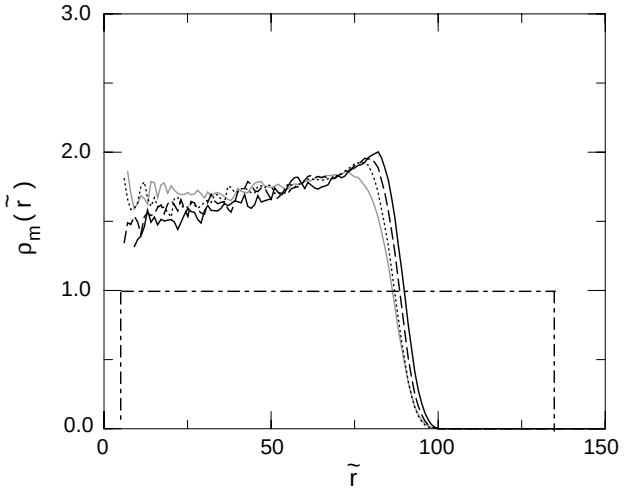

Fig. 11. Monomer density profiles for $\zeta = 2$, $N = 130$ and $f = 6$ (dotted line), $f = 27$ (dashed line), and $f = 54$ (full black line). They are compared to the density profile of a free polyelectrolyte branch with $R_{\rm core} = 0$ and $f = 1$ (gray line). Since $R_{\rm c} = 5a$ for all other curves, this last gray line has been translated by 5 units in the x-direction. The dot-dashed line indicates the profile corresponding to fully extended branches. Only a slight increase of the corona radius is observed when the number of branches is varied by a factor 10 (from $f = 6$ to $f = 54$).

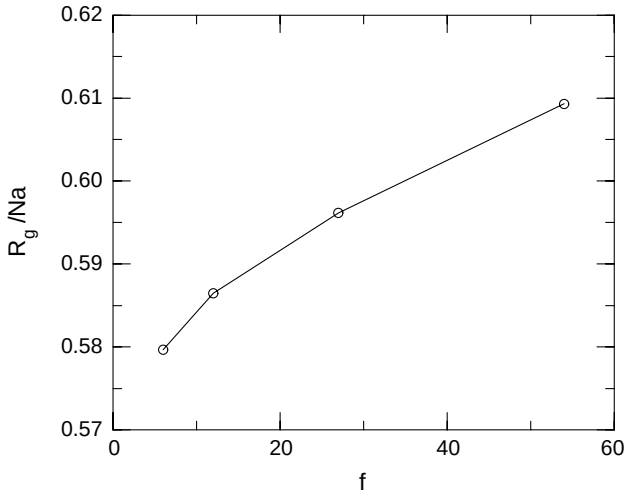

Fig. 12. Variation of the gyration radius $R_{\rm g}$ as a function of the number of branches f for $\zeta = 2$ and $N = 130$. Only an increase of a few percent of $R_{\rm g}$ is observed when the number of branches is varied by a factor 10.

factor of 10. The MD results of JLL (see Tabs. I and II in Ref. [8]), also show a weak dependence of $R_{\rm c}$ on f.

Figure 13 represents a blow up over the last 80 monomers of one branch in Figure 4c. At a length scale of the order of 10 monomers, a local "rod-like" picture is relevant. To illustrate the phase space explored by a given branch, we have registered 100 snapshots of the same branch (Fig. 14), at equal time intervals in thermodynamic equilibrium. The phase space explored corresponds

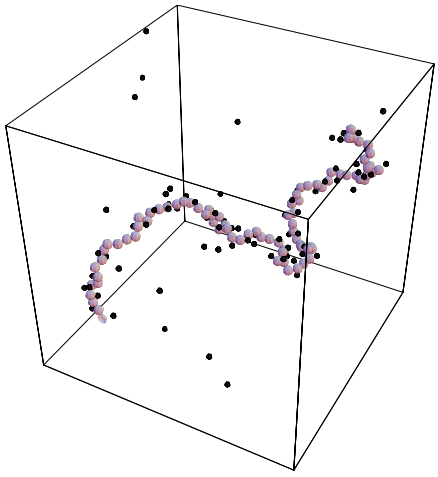

Fig. 13. A blow up over the last 80 monomers of one branch in Figure 4c. Large spheres are fully charged monomers. Small spheres with diameter 1/2 of the large ones are counterions.

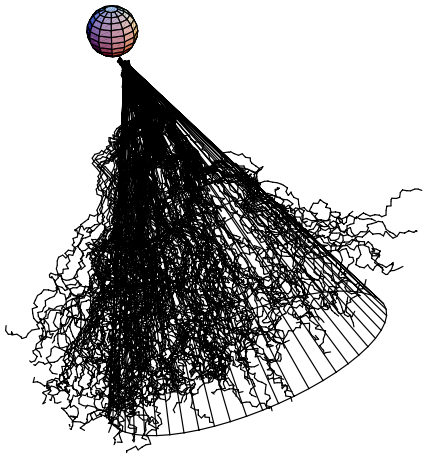

Fig. 14. Snapshots of the same branch at equal time intervals during measurement of thermodynamic quantities. The portion of space explored corresponds to a cone of solid angle $4\pi/f$ steradians. The sphere at the top represents the hydrophobic core.

roughly to a cone of solid angle $4\pi/f$ steradians which shows that each branch occupies a fraction $1/f$ of the sphere and rarely "mixes" with neighboring branches. An "urchin-like" picture [22] is thus relevant.

The last decade in Figure 5 and its enlargement in Figure 10 show that, in our fully charged model ($\alpha = 1$), beyond the Manning threshold, the corona radius $R_{\rm c}$ decreases roughly in $\zeta^{-1/3}$. This decrease of $R_{\rm c}$ as well as its independence from f can be interpreted with the following simple arguments.

For $\zeta > 1$, there is a cylindrical condensation of a fraction of counterions along the branches. The model proposed by Manning [10], considers that a fraction $(1 - 1/\zeta)$ of the counterions condenses around the branches in such a way that the monomers get an effective charge $\alpha_{\rm eff} z_{\rm m}$ with an effective charge fraction

$$\alpha_{\rm eff} = 1/\zeta. \qquad (12)$$

The remaining fraction $1/\zeta$ of counterions are only spherically condensed and distributed between the branches. We assume that f is sufficiently high ($\zeta \gg 1/f$) to neglect the fraction of "free" counterions outside the corona. Taking a spherical distribution in $1/r^2$, we obtain the following effective ion density:

$$c_{\rm i}^{\rm eff}(\tilde{r}) = \frac{1}{\zeta}\frac{fN}{4\pi a^2 R_{\rm c}\tilde{r}^2}\frac{|z_{\rm m}|}{|z_{\rm i}|}. \tag{13}$$

The corresponding "effective" screening length is

$$\kappa_{\rm eff}^{-1}(\tilde{r}) = [4\pi l_{\rm B} z_{\rm i}^2 c_{\rm i}^{\rm eff}]^{-1/2} = a\tilde{r}\left[f\frac{Na}{R_{\rm c}}\right]^{-1/2}. \tag{14}$$

It depends only weakly on ζ through $R_{\rm c}^{1/2}$ and roughly keeps the value it reaches at the Manning condensation threshold $\zeta = 1$. At a radial position r, the mean transverse distance between two neighboring branches is roughly $4a\tilde{r}f^{-1/2}$. It exceeds the screening length by a factor of the order of 4. Hence we can neglect the electrostatic interactions between branches. Since the polymers are relatively extended, the excluded-volume interactions between branches are also weak. This is the reason why the monomer profiles are so weakly dependent on f.

The osmotic pressure of these spherically condensed counterions decreases as $1/\zeta$. The effective Coulomb repulsion between two monomers at distance r,

$$k_{\rm B}T\alpha_{\rm eff}^2 z_{\rm m}^2 (l_{\rm B}/a){\rm e}^{-\kappa r} = k_{\rm B}T\zeta^{-1}\frac{|z_{\rm m}|}{|z_{\rm i}|}{\rm e}^{-\kappa r} \tag{15}$$

also decreases as $1/\zeta$. Both effects contribute to a decrease of $R_{\rm c}$.

More quantitatively, we can consider one branch in the familiar electrostatic "blob" picture [13,23]. A branch is represented as a succession of N/g Pincus blobs of size $\xi_{\rm P}$, each containing g monomers. The size $\xi_{\rm P}$ of a blob is such that the energy corresponding to the sum F of electrostatic and/or other forces acting on it is of the order of $k_{\rm B}T$:

$$F\xi_{\rm P} \approx k_{\rm B}T. \tag{16}$$

Inside a blob, the energy corresponding to these forces is less than $k_{\rm B}T$ and the behavior of the corresponding part of the chain can be considered as roughly Gaussian *i.e.*:

$$\xi_{\rm P}^2 \approx g a^2\,. \tag{17}$$

The repulsive force between two blobs tends to align them and we have $R_{\rm c} = (N/g)\xi_{\rm P}$. Taking equation (17) into account, we can write

$$R_{\rm c}/(Na) = a/\xi_{\rm P}. \tag{18}$$

In the ζ range that we consider, $Na/R_{\rm c}$ is close to 2. Hence $\xi_{\rm P}$ is of the order of $2a$ and each blob contains roughly 4 monomers. Here the force F acting on a blob is the sum of two contributions:

i) The electrostatic force due to unscreened short-range Coulomb repulsion between monomers with effective charge $\alpha_{\rm eff} z_{\rm m} e$ in a blob:

$$F_{\rm c} = k_{\rm B}T(g\alpha_{\rm eff})^2\frac{a}{\xi_{\rm P}^2}\frac{|z_{\rm m}|}{|z_{\rm i}|}\zeta. \tag{19}$$

This relation is valid for $\kappa^{-1} > \xi_{\rm P}$, *i.e.* from equations (14) and (18) for a radial distance $\tilde{r} > \sqrt{f}(Na/R_{\rm c})^{3/2}$. For $\zeta \approx 4$, $Na/R_{\rm c}$ is of order 2 and with $f = 27$ this corresponds to $\tilde{r} > 15$. At a radial distance r between $R_{\rm core}$ and $\approx 15a$, the size of the blob depends on r. This region is however sufficiently narrow for this effect to be neglected as a first approximation.
Since $\alpha_{\rm eff} = 1/\zeta$ and $|z_{\rm m}| = |z_{\rm i}|$, we have

$$F_{\rm c} = k_{\rm B}T\frac{ag^2}{\xi_{\rm P}^2}\zeta^{-1}. \tag{20}$$

ii) The force due to the osmotic pressure of the fraction $1/\zeta$ of counterions which are only spherically condensed in the corona. This force is constant all along the chain:

$$F_{\rm osm} = k_{\rm B}T(N/R_{\rm c})\zeta^{-1}. \tag{21}$$

Substituting $F = F_{\rm c} + F_{\rm osm}$ in equation (16) leads to

$$\frac{ag^2}{\xi_{\rm P}}\zeta^{-1} + N\frac{\xi_{\rm P}}{R_{\rm c}}\zeta^{-1} = 1. \tag{22}$$

From equations (17, 18) and (22) we deduce the following relation for $R_{\rm c}$:

$$\left(\frac{Na}{R_{\rm c}}\right)^3\zeta^{-1} + \left(\frac{Na}{R_{\rm c}}\right)^2\zeta^{-1} = 1. \tag{23}$$

Taking only into account the second term in the left-hand side of equation (23) corresponds to the approximation usually made in the "osmotic regime" [2,3] (see the last paragraph of Sect. 3.4) and would lead to a decrease of $R_{\rm c}$ in $\zeta^{-1/2}$. However, even near the maximum of $R_{\rm c}$ at $\zeta \approx 1$, where $Na/R_{\rm c} \approx 1.3$, the first term which takes into account the unscreened short-range Coulomb repulsion between monomers is of the same order. At large $\zeta \gg 1$, *i.e.* $Na/R_{\rm c} \gg 1$, this term dominates and leads to a decrease of $R_{\rm c}$ in $\zeta^{-1/3}$ [24]. At $\zeta > 4$, this term is already twice as large as the second one and the overall behavior of the solution of equation (23) is close to $R_{\rm c}/(Na) \approx \zeta^{-1/3}$, as observed in our Monte Carlo simulation (see Fig. 10).

At high ζ, Schiessel and Pincus [23] predicted a collapse of the polymers with the following arguments. When the Coulomb energy dominates over the entropic contribution, each counterion is practically fixed to a monomer and forms an electric dipole. The attraction of dipoles should lead to a transition towards a collapse of the star. Up to $\zeta = 10$, our results follow the same $\approx \zeta^{-1/3}$ power law, and we do not observe any precursor of this effect.

The Manning picture allows us to propose some approximate mapping of our model at $\alpha = 1$, $\zeta = 3$ onto

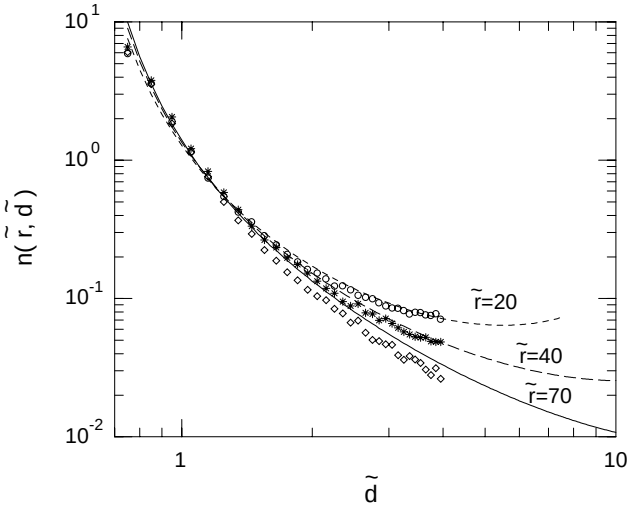

Fig. 15. Density of counterions at a radial distance $\tilde{r}$ from the micelle center and a transverse distance from the nearest branch $\tilde{d}$. The results of the Monte Carlo simulation (symbols) are compared to those of a Poisson-Boltzmann approximation (lines). Circles and short-dashed line: $\tilde{r} = 20$; stars and long-dashed line: $\tilde{r} = 40$; diamonds and full line: $\tilde{r} = 70$. Here, $\zeta = 3$, $N = 130$, $f = 27$ and $\tilde{A} = 320$.

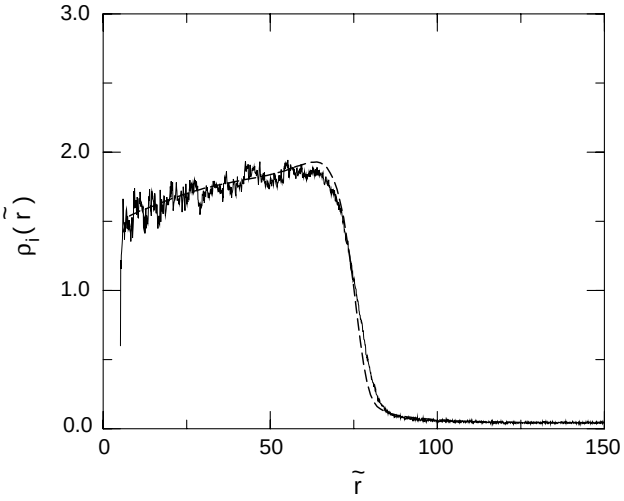

Fig. 16. Radial density of counterions. The Monte Carlo results are compared to the Poisson-Boltzmann approximation (dashed line). Here, $\zeta = 3$, $N = 130$, $f = 27$ and $\tilde{A} = 320$.

the model of JLL at $\alpha = 1/3$ and the same $\zeta = 3$. In our model, at $\zeta = 3$, due to Manning condensation, $(1 - 1/\zeta) = 2/3$ of the counterions condense on the monomers. The remaining effective charge fraction of monomers is thus $\alpha_{\rm eff} = 1/3$ and the other one third of the counterions is only spherically condensed inside the corona. This effective model is thus close to the real situation studied by JLL at $\alpha = 1/3$ and $\zeta = 3$. The arrow in Figure 10 shows a very nice agreement of the corona radii corresponding to this mapping. This is a strong evidence of the relevance of Manning's picture.

Up to now, radial distributions of counterions were only considered. In the Manning regime, it is of prime interest to study the cylindrical distribution of counterions around one branch. Defining the distance d of a counterion to the closest branch as the distance to the closest monomer, we have measured the mean value of the radial density $n(r, d)$, $n(r, d)\delta r\delta d$ representing the number of counterions at distance between d and $(d + \delta d)$ from a branch and at radial distance between r and $(r + \delta r)$ from the center of the micelle.

Figure 15 represents the density $n(\tilde{r}, \tilde{d})$ of counterions at distance $d = \tilde{d}a$ from the closest branch and at a distance $\tilde{r}a$ from the center of the micelle for three values of $\tilde{r}$: close to the core ($\tilde{r} = 20$), in the middle ($\tilde{r} = 40$) and close to the edge of the corona ($\tilde{r} = 70$). We chose $\zeta = 3$, well above the Manning threshold, $N = 130$, $f = 27$ and $\tilde{A} = 320$.

It is interesting to compare these results to those expected from a "rod-like" picture of the arms and a Poisson-Boltzmann approach for the distribution of counterions.

Using the "FIDISOL/CADSOL" package developed at Rechenzentrum, Universität Karlsruhe [25] for the numerical solution of non-linear partial differential equations, we have solved the Poisson-Boltzmann equation for a rod in a cone of solid angle $(4\pi/f)$. The radius of the rod is chosen to $0.75a$, which corresponds to the sum of the hard-core radii of monomer and counterion. The height of the cone is equal to the radius of a sphere of volume A^3. The distribution of charges in the rod corresponds to the monomer profile obtained in Figure 3c through Monte Carlo simulation. (In practice, we fit this distribution to an approximation by a rational function.) Using a two-dimensional 80×120 grid, we obtained an accuracy better than 10^{-4} on almost every point. The calculation took only one minute of monoprocessor time. There is a nice agreement except in the vicinity of the corona radius.

Figure 16 compares the overall density profile $\rho_{\rm i}(\tilde{r})$ obtained through the Poisson-Boltzmann approach to the Monte Carlo results of Figure 3c.

An interesting quantitative way to characterize the Manning threshold is to plot in log-linear coordinates the number $\nu_{\rm i}(\tilde{d})$ of counterions at a distance less than $\tilde{d}$ from the closest monomer (*i.e.* the integral over $\tilde{d}'$ of $n(\tilde{r}, \tilde{d}')$ between 0.75 and $\tilde{d}$) [16]. Within the Poisson-Boltzmann approximation, $\nu_{\rm i}(\tilde{d})$ is expected to follow a logarithmic law at the Manning threshold [15]. As shown in Figure 17, there is a change of curvature of the lines between $\zeta = 0.5$ and $\zeta = 1.5$. A straight line (logarithmic behavior) is obtained at $\zeta = 1$.

Figure 18 shows that, in the Manning condensed regime, $\nu_{\rm i}(\tilde{d})$ is practically independent of the boundary conditions: the results obtained after doubling the size of the cubic cell ($\tilde{A} = 640$) are practically identical to those obtained with $\tilde{A} = 320$. $\nu_{\rm i}(\tilde{d})$ depends on the number of arms but the threshold value $\zeta_{\rm M} \approx 1$ corresponding to Manning condensation is unchanged.

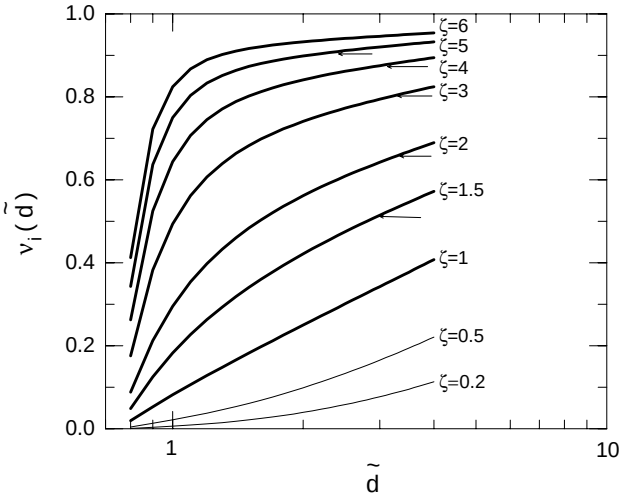

Fig. 17. Number $\nu_i(\tilde{d})$ of counterions per monomer at a distance less than d from the closest branch, for different values of the dimensionless parameter ζ. Here $N = 130$, $f = 27$ and $\tilde{A} = 320$. The change of curvature between $\zeta = 0.5$ and $\zeta = 1.5$ corresponds to Manning condensation. The Manning threshold $\xi = 1/z_i$ is reached at $\zeta \approx 1$. A logarithmic dependence of ν on $\tilde{d}$ is expected at $\xi = 1/z_i$, from a Poisson-Boltzmann approximation in a "rod-like" picture. For each value of ζ in the Manning condensed regime, the arrow indicates the distance at which the "effective charge parameter" $\alpha_{\rm eff} = 1 - \nu_i$ leads to $\xi_{\rm eff} = 1/z_i$.

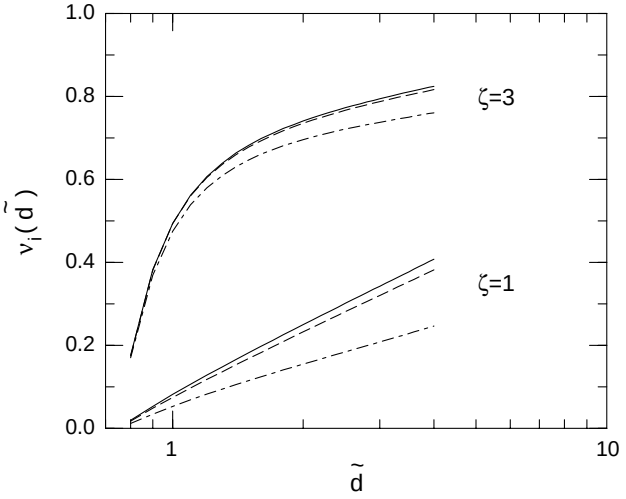

Fig. 18. Dependence of $\nu_i(\tilde{d})$ on the number of arms f and boundary conditions (size $\tilde{A}$ of the cubic cell). Full lines: $N = 130$, $f = 27$ and $\tilde{A} = 320$; dashed lines: $N = 130$, $f = 27$ and $\tilde{A} = 640$; dash-dotted lines: $N = 130$, $f = 6$ and $\tilde{A} = 640$.

4 Simulation of an experimental system

4.1 Description of the experimental system

We used asymmetric diblock copolymers made of fully deuterated sodium poly-(styrene-sulfonate)($\rm NaPSS_d$) and of (polyethylene-propylene)(PEP) [9]. These materials were synthetized by anionic polymerization. The degrees of polymerization were measured and found to be 251 for ($\rm NaPSS_d$) moiety and 52 for (PEP) moiety. The aggregation number, *i.e.* the number of branches per micelle, was found to be 54 and the core radius is $R_{\rm core} \approx 4.5$ nm $\approx 18a$. The monomer size for ($\rm NaPSS_d$) moieties is $a = 0.25$ nm. Taking $l_B = 0.71$ nm as the Bjerrum length of pure water at room temperature, the dimensionless parameter ζ is evaluated to $\zeta = l_B/a = 2.8$. The concentration is $0.25c^*$ where c^* represents the overlap concentration. Our cubic cell was chosen such that its volume represents the mean volume occupied by one micelle in the solution, *i.e.* $\tilde{A} = 560$.

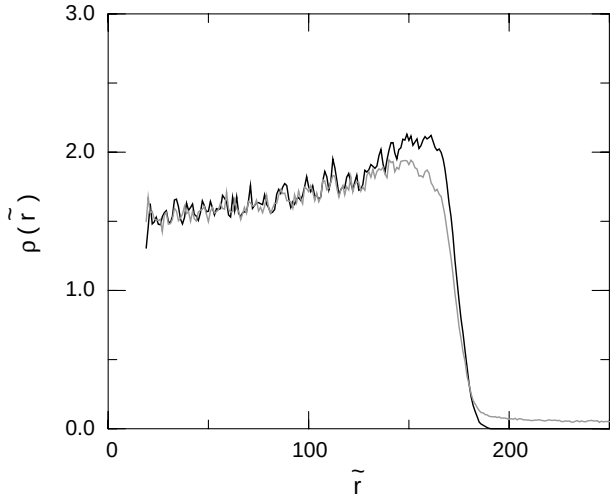

Fig. 19. Density profiles of monomers (black line) and counterions (gray line) for a micelle with 54 branches of 251 monomers at $\zeta = 2.8$ with $R_{\rm core} = 18a$ and $\tilde{A} = 560$.

4.2 Monomer and counterion profiles

The density profiles of monomers and counterions are plotted in Figure 19. The corona radius is $R_c = 174a$ leading to $(R_c - R_{\rm core})/Na \approx 0.62$; this value has to be compared to that obtained in Section 3 with $N = 130$ and $f = 54$ at the same ζ: $(R_c - R_{\rm core})/Na \approx 0.57$. We agree with the Molecular-Dynamics results of JLL [7,8] on smaller branch lengths showing that the ratio R_c/N is not strictly constant but slightly decreases when N increases. The monomer and ion profiles are quite similar to those observed in Section 3 for $N = 130$ and $f = 27$ (compare with Fig. 3c).

4.3 Form factor, comparison to experimental results

The monomer-monomer form factor obtained through the Monte Carlo simulation, with the parameters described in Section 4.1 is shown in Figure 20 (thick dash-dotted line). It is close to the monomer-monomer form factor obtained through neutron scattering [9] except in the range $q \approx \pi/R_{\rm core}$, where the size of the core has a large influence on the spectrum. Another Monte Carlo calculation with

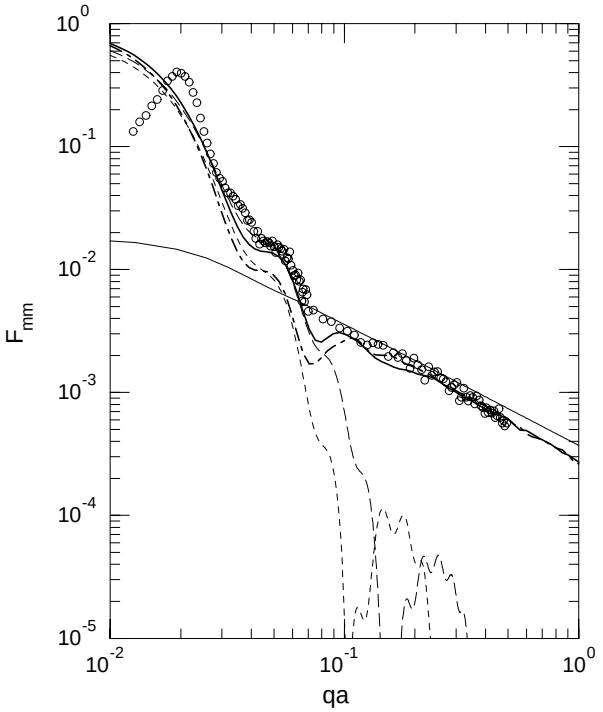

Fig. 20. Monomer-monomer form factor for a micelle with 54 branches of 251 monomers at $\zeta = 2.8$. The experimental results (circles) are compared to two Monte Carlo calculations with different core size (all other parameters being the same): i) thick full line: $R_{\rm core} = 12a$; ii) thick dash-dotted line $R_{\rm core} = 18a$. The thin lines indicate analytical asymptotic behaviors. Thin full line: the form factors of perfect rods of length $R_{\rm c} - R_{\rm core}$; Thin long-dashed and short-dashed lines: the form factors for spherical distributions of monomers in $1/r^2$ between $R_{\rm core}$ and $R_{\rm c}$ for $R_{\rm core} = 12a$ and $R_{\rm core} = 18a$, respectively.

a slightly smaller core $R_{\rm core} = 12a$ (thick full line) was performed. It is in a better agreement with the neutron scattering results.

It is interesting to compare the simulated and experimental results to straightforward analytical approximations at low and high q.

At low q, ($q < \pi/R_{\rm core}$), the form factor can be reasonably approximated by that of a $1/r^2$ spherical distribution of monomers from $r = R_{\rm core}$ to $r = R_{\rm c}$ and zero otherwise:

$$F^{\rm sph}(q) = \left[\frac{{\rm Si}(qR_{\rm c}) - {\rm Si}(qR_{\rm core})}{qR_{\rm c}}\right]^2, \qquad (24)$$

where ${\rm Si}(z)$ represents the Sine-Integral function [26]. The thin long-dashed and short-dashed lines represent this function for $R_{\rm core} = 12a$ and $R_{\rm core} = 18a$, respectively. Up to $qa \approx 0.1$ they closely follow the corresponding Monte Carlo simulations (thick full and dash-dotted lines). At $q \approx \pi/R_{\rm core}$ large oscillations appear in the function $-{\rm Si}(qR_{\rm core})$, the first of them being responsible for a dip observed in the simulation. Close to this dip, the form factor is very sensitive to the size of the core. We find that our simulation with $R_{\rm core} = 12$ is closer to the experimental results than that with $R_{\rm core} = 18$. The interface between the hydrophobic core and the hydrophilic branches might happen to be not so smooth and as well defined as assumed in our model. For example, some hydrophilic monomers may be trapped inside the outer part of the core, leading to a lower effective core radius.

At high q, the branches can be approximated by rods of length $L = R_{\rm c} - R_{\rm core}$ with negligible thickness. The corresponding form factor is

$$F^{\rm rod}(q) = \frac{1}{f}\left\{\frac{2}{qL}{\rm Si}(qL) - \left[\frac{\sin(qL/2)}{qL/2}\right]^2\right\}. \qquad (25)$$

The thin full line represents this function with $L = R_{\rm c} - R_{\rm core} = 156a$ corresponding to our Monte Carlo estimate. At large q, $F^{\rm rod}(q) \approx [1/fq(R_{\rm c} - R_{\rm core})]$ and the position of this line of slope (-1) in logarithmic coordinates gives a nice estimate of the corona radius. In conclusion, the corona radius obtained through our Monte Carlo simulation is in agreement with the experimental value.

The peak observed in the experimental data at $qa \approx 0.02$ arises from long-range correlations between micelles, mostly due to the remaining uncondensed charges. It is a collective effect which, of course, is absent in our model. The concentration is $c = 5 \times 10^{-3}{\rm g/cm}^3$. The corresponding q wave vector characterizing the inter-micelle correlations is $q \approx 2\pi[c\mathcal{N}/fM]^{1/3}$, where $M = 5.7 \times 10^4$ is the molar mass of one diblock copolymer and $\mathcal{N}$ the Avogadro number. We obtain $qa \approx 0.016$ in reasonable agreement with the position of the peak.

5 Conclusion

Monte Carlo simulations appear to be a useful tool for understanding the complex structure of highly charged copolymer urchin-like micelles. As the Coulomb coupling is increased, three different regimes can be distinguished. i) At low coupling, the freely jointed polyelectrolyte branches become stretched due to the monomer-monomer repulsion and the micelle swells. The monovalent counterions are not sensitive to the low micellar charge and are uniformly distributed inside the cell. ii) At intermediate coupling, the arms are almost fully stretched and most of the counterions are trapped inside or in close vicinity of the micelle. This spherical condensation is due to the presence of many, although weakly charged, branches in the same micelle. iii) At large coupling, a classical ionic condensation appears locally around each highly charged branch which adds to the previous one. The effective post-condensation monomer charge decreases, the monomer-monomer repulsion weakens and the micelle deswells. These Monte Carlo results agree with Poisson-Boltzmann analyses in different geometries and nicely reproduce small-angle neutron scattering data. The influence of intrinsic chain rigidity, and the role of ion-ion correlation in presence of multivalent counterions will be investigated in future papers.

References

1. O.V. Borisov, E.B. Zhulina, J. Phys. II **7**, 449 (1997).
2. O.V. Borisov, E.B. Zhulina, Eur. Phys. J. B **4**, 205 (1998).
3. J. Klein Wolterink, F.A.M. Leermakers, G.J. Fleer, L.K. Koopal, E.B. Zhulina, O.V. Borisov, Macromolecules **32**, 2365 (1999).
4. G.S. Grest, K. Kremer, T.A. Witten, Macromolecules **20**, 1376 (1987).
5. M.J. Stevens, K. Kremer, J. Chem. Phys. **103**, 1669 (1995).
6. U. Micka, C. Holm, K. Kremer, Langmuir, **15**, 4033 (1999).
7. A. Jusufi, C.N. Likos, H. Löwen, Phys. Rev. Lett. **88**, 018301 (2002).
8. A. Jusufi, C.N. Likos, H. Löwen, J. Chem. Phys. **116**, 11011 (2002).
9. F. Muller, M. Delsanti, L. Auvray, J. Yang, Y.J. Chen, B. Demé, M. Tirrell, P. Guenoun, Eur. Phys. J. E **3**, 45 (2000).
10. G.S. Manning, J. Chem. Phys. **51**, 924 (1969).
11. L. Belloni, Colloid Surf. A **140**, 227 (1998).
12. P. Pincus, Macromolecules **24**, 2912 (1991).
13. P.G. De Gennes, P. Pincus, R.M. Velasco, F. Brochard, J. Phys. (Paris) **37**, 1461 (1976).
14. P. Guenoun, F. Muller, M. Delsanti, L. Auvray, Y.J. Chen, W.J. Mays, M. Tirell, Phys. Rev. Lett. **81**, 3872 (1998).
15. R.M. Fuoss, A. Katchalsky, S Lifson, Proc. Natl. Acad. Sci. USA **37**, 519 (1951).
16. L. Belloni, M. Drifford, P. Turq, Chem. Phys. **83**, 147 (1984).
17. N. Madras, A.D. Sokal, J. Stat. Phys. **50**, 109 (1988).
18. H.L. Gordon, J.P. Valleau, Mol. Sim. **14**, 361 (1995)
19. V. Lobaskin, P. Linse, J. Chem. Phys. **111**, 4300 (1999).
20. M. Daoud, J.P. Cotton, J. Phys. (Paris) **43**, 531 (1982).
21. JLL consider $b = R_c/(N\alpha)$ rather than $b = a/\alpha$. The relevant question is: how to extend the Manning concepts from a perfect cylindrical rod to a wiggling chain. We consider that the cylindrical picture remains valid at small length scale (of the order of ten monomers) and that our local definition $b = a/\alpha$ is more relevant than the global one $b = R_c/(N\alpha)$, which incorporates the large-scale wiggles of the chain shown in Figure 13 (see Ref. [24]). Nevertheless, taking $b = R_c/(N\alpha)$ instead of $b = a/\alpha$ merely shifts in Figure 10 the data of JLL as well as ours from a factor Na/R_c and does not affect our general discussion.
22. F. Muller, M. Delsanti, L. Auvray, J. Yang, Y.J. Chen, J.W. Mays, B. Demé, M. Tirrell, P. Guenoun, Eur. Phys. J. E **6**, 109 (2001).
23. H. Schiessel, P. Pincus, Macromolecules **31**, 7953 (1998).
24. If we neglect the entropy of counterions, this blob picture in the "Manning condensed" regime, with effective charge renormalization, is identical to that proposed by Schiessel and Pincus [23] for dilute solutions of polyelectrolytes, except that we consider a renormalizing factor: $\alpha_{\rm eff} = 1/\zeta = a/l_B$, while their equation (2) corresponds, with our notations, to $\alpha_{\rm eff}^{\rm SP} = (R_c/N)/l_B$ and leads to the exponent -1 instead of $(-1/3)$. We are left with the same question as the one risen in reference [21] about how to define the "Manning parameter" for an imperfect rod. In Figure 10, our Monte Carlo results for R_c roughly show, at high ζ, a $(-1/3)$ exponent. This indicates that our "local" picture is more relevant.
25. R. Weiss, M. Schmauder, W. Schönauer, Rechenzentrum, Universität Karlsruhe, `http: //www.uni-karlsruhe.de /Uni/RZ/Forschung/Numerik`.
26. M. Abramowitz, I.A. Stegun, *Handbook of Mathematical Functions*, (National Bureau of Standards, Washington D.C., 1964).